Combining Magnets and Dielectrics: Crystal Chemistry in the $BaO-Fe_2O_3-TiO_2$ System

Theo Siegrist*[a][‡] and Terrell A. Vanderah[b]

Keywords: Dielectric properties / Magnetic properties / Perovskite phases / Solid-state structures / Titanates / Ferrites

Phases observed in the $BaO–Fe_2O_3–TiO_2$ system are classified and described in terms of the framework of close-packed {O,Ba/O} layers, with the transition metal atoms either in octahedral (titanium and iron) or in tetrahedral (iron only) sites. The resulting crystal chemistry features new combinations of structural features intermediate between the magnetic barium hexaferrites and the dielectric barium polytitanates, and thus gives rise to phases with potentially useful magnetic/dielectric properties.

1. Overview

The crystal chemistry in the $BaO-Fe_2O_3-TiO_2$ phase diagram is surprisingly rich. A recent study of the system found a large number of new phases,[1] with structures featuring moieties from both the polytitanates and hexaferrites, as well as new building blocks showing a mixture of features from both. The observed structural features organize the composition space into regions containing phases with common building units. These regions in the phase diagram, as indicated in Figure 1, include those featuring framework-type structures (e.g., hollandites, indicated in yellow), the perovskite derivatives and polytitanates (light blue), the hexaferrites (dark blue), and intermediate phases with new structural units (red). Magnetic multilayer compounds are in the violet/gray area. The areas are defined by bisecting existing tie lines and are a guide to the eye.

As can be seen, three distinct "structural end members" ($BaO-TiO_2$, $Fe_2O_3-TiO_2$, and $BaO-Fe_2O_3$) dominate along the binary subsystems. The framework-type structures such as hollandite dominate the lower left corner of

[a] Bell Laboratories, Lucent Technologies
600 Mountain Avenue, Murray Hill, NJ 07974, USA
[b] Ceramics Division, Materials Science & Engineering Laboratory, National Institute of Standards and Technology
Gaithersburg, MD 20899, USA
[‡] Second address: Materials Chemistry, Lund University, 22100 Lund, Sweden.

Theo Siegrist was born in Winterthur, Switzerland. He received his diploma in physics (Dipl.-Phys. ETH) from the Federal Institute of Technology (ETH) in Zürich in 1979. He then enrolled in the Ph.D. program at the Laboratory for Solid State Physics at ETH, working in the area of rhenium intermetallic compounds with F. Hulliger. He was awarded the Dr. sc. nat. in 1982. In 1983 he joined the group of F. Holtzberg at the IBM T. J. Watson Research Center as a postdoctoral fellow, working on thin films of semimagnetic semiconductors. In 1985 he became a research associate at the National Research Council of Canada in Ottawa, in the Solid State Chemistry department. There he investigated rare earth intermetallics and heavy fermion uranium compounds. He joined Bell Laboratories in New Jersey, USA in 1986, where he entered the field of high T_c superconductors based on copper oxides. He investigated the crystal chemistry of this new class of compounds and related phases. Further work was done on C_{60} and its compounds, various oxides, and intermetallic phases. From 1998 he spent two years as Professor of Solid State Chemistry at Lund University/Lund Institute of Technology, where he investigated new phases with mixed anion lattices. From 2000 he has once again been at Bell Labs, working on the structural characterization of organic electronic materials and on the crystal chemistry of new phases.

Terrell Vanderah received a B.S. in Chemistry from the University of Maryland in 1977 and a Ph.D. in Inorganic (Solid State) Chemistry from the University of Connecticut in 1985, with Prof. B. L. Chamberland. From 1985 to 1993 she worked as a research chemist at the Naval Weapons Center in China Lake, California, in the area of non-oxide optical ceramics and high-temperature superconductors. In 1994 she moved to the National Institute of Standards and Technology in Gaithersburg to become the group leader for Phase Equilibria. Her research interests include the solid-state chemistry and phase equilibria of oxide systems of electronic interest and the interrelationships of crystal structure, chemical composition, and properties.

MICROREVIEWS: This feature introduces the readers to the author's research through a concise overview of the selected topic. Reference to important work from others in the field is included.

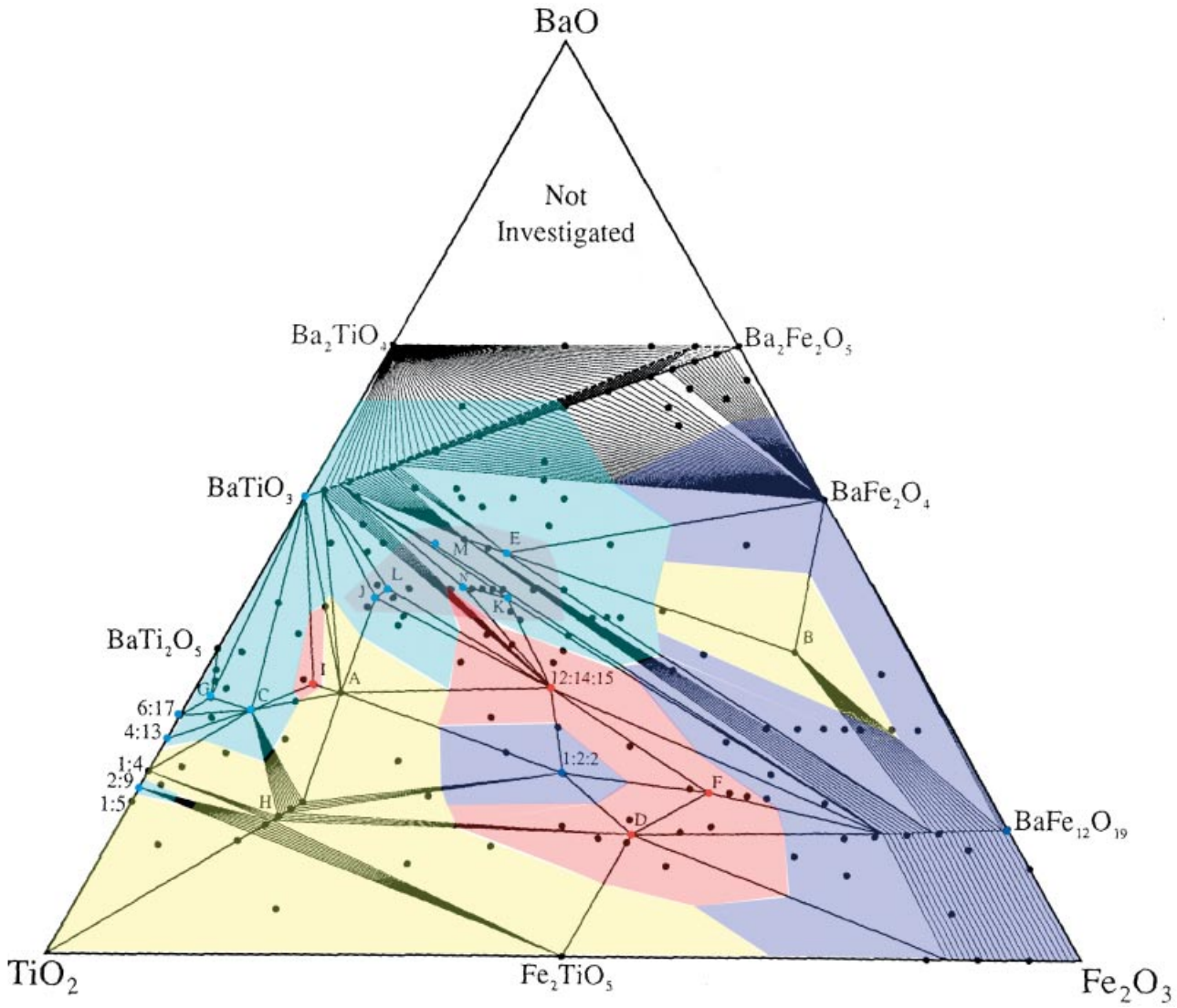

Figure 1. $BaO-Fe_2O_3-TiO_2$ phase diagram with regions of structurally related phases indicated in color; yellow: framework-type phases; light blue: hexagonal polytitanates; dark blue: hexaferrites; violet/gray: magnetic multilayer systems (based on hexagonal perovskite and hexaferrite); red: new "mixed" phases

the phase diagram nearest TiO_2. The other two structural "end members", the polytitanates/perovskites (Ti-rich side) and hexaferrites (Fe-rich side), both feature close-packed {O,Ba/O} layers and would therefore be expected to form numerous "blended" structures. Indeed, in the transition area indicated in red, the phases found are based on seven new types of close-packed {O,Ba/O} layers intermediate between the layers present in the hexaferrites and in the polytitanates. The stacking of the different layers gives rise to a variety of phases, extending from the iron-rich to the titanium-rich side. Phases in this region based on hexagonal $BaTiO_3$ with Fe ordering in distinct layers reveal superstructures with periodicities of around 100 Å. Disorder in stacking is often seen, but their structural features are similar to the other intermediate phases.

Phases indicated in violet/gray include blocks of hexagonal $BaTiO_3$ and often disordered layers mainly comprised of $BaO-Fe_2O_3$.[2] These phases are part of the red area of new structures.

The structural features observed in the $BaO-Fe_2O_3-TiO_2$ system are presented below, and some of the new phases found are discussed. The combination of high dielectric and ferri-/ferromagnetic systems produces potentially useful materials for microwave applications, such as nonreciprocal devices.[3,4] The dielectric properties of some of the phases are discussed in terms of the Clausius–Mosotti theory. Furthermore, the iron valence has to be stabilized at Fe^{3+} to ensure low microwave losses. The phases discussed below are based on Fe^{3+} and Ti^{4+}.

2. Background

High dielectric materials have been key in the miniaturization of microwave devices (i.e. high frequencies of the

order of 50 MHz to 22 GHz). Use of a dielectric material allows the size of a microwave device to be scaled by $\varepsilon^{-1/2}$. Requirements for materials used in microwave applications are a high dielectric constant and low microwave losses, together with a negligible temperature dependence of these properties. Materials in common use are based on mixtures of barium titanates, in which dielectric constants of the order of 28, together with small temperature dependencies, are observed. Furthermore, microwave losses can be reduced such that high-quality filters with Q of the order of 45k and higher can be realized. The loss mechanisms are often related to defects in the material; the presence of reduced titanium, Ti^{3+}, for instance, correlates with increased loss. Careful synthesis of the material to ensure fully oxidized titanium is key to performance.

The addition of a static magnetic field affects the propagation of the electromagnetic wave in such a material, allowing the construction of nonreciprocal devices such as isolators, phase shifters, circulators, etc. Such ceramic magnetic oxides are key components in a wide variety of electronic applications; communication systems, for instance, utilize coaxial circulators and isolators that contain ceramic magnets.[3,4] Materials in current use include spinels, garnets, and hexaferrites, the last of these based on the magnetoplumbite-type structure. Improved materials would exhibit higher dielectric constants and high saturation magnetization, while retaining low-loss behavior in the microwave region. In addition, a small or negligible temperature dependence of the dielectric and magnetic properties is highly desirable. For this reason, a thorough study of the phase equilibria in the $BaO-Fe_2O_3-TiO_2$ system was recently carried out.[1] In particular, combinations of the high dielectric materials based on polytitanates with magnetic Fe_2O_3 were of interest. Since the materials in use today are often based on mixtures of several different crystallographic phases, detailed knowledge of the phase diagram is key to understanding the processing of multicomponent materials with engineered properties. The interface of the barium hexaferrites with the barium polytitanates is discussed below, and the structural relationships emphasized.

The pseudo-binary systems have been examined previously, and corresponding phase diagrams were produced in "Phase Equilibria Diagrams" (formerly "Phase Diagrams for Ceramists"),[5] in Figures 1:208, 4:5130, 91:009, 1:213, 3:4302, 4:5135, 11:9211–13, 93:016, 12:10036, and references cited therein.

The crystal chemistries both of the barium polytitanates[6] and of the barium hexaferrites[7] have been extensively studied in the past. These systems are based on close-packed oxygen lattices, with barium atoms substituting for oxygen atoms while retaining the close-packed arrays. Titanium and iron atoms occupy interstitial sites. The resulting structures obey a metric determined by the close-packed lattice, usually based on a hexagonal unit cell, with layers approximately 2.35 Å thick and in-plane base hexagonal lattice parameters of the order of $a = b = 5.75$ Å. Ordering of the transition metal atoms in interstitial sites and of the barium atoms which are substituted for oxygen atoms often reduces symmetry from hexagonal or rhombohedral to orthorhombic or monoclinic, and correspondingly changes the in-plane lattice parameters. The similar unit cell metrics of the two systems allow the formation of mixed or "blended" phases that would be expected to contain structural motifs both from the polytitanates and from the hexaferrites, giving rise to new structures. Furthermore, new structural motifs combining features of both end systems may also occur.

Only one phase is stable in the pseudobinary $Fe_2O_3-TiO_2$ system: pseudobrookite-type Fe_2TiO_5. It may be regarded as a framework-type structure with edge-sharing octahedra only.

The barium polytitanates may be described as $(BaO)_m(TiO_2)_n$. Of the six phases stable above 1200 °C in the $BaO-TiO_2$ system, $Ba_2Ti_9O_{20}$,[8] $BaTi_4O_9$,[9] $Ba_4Ti_{13}O_{30}$,[10] $Ba_6Ti_{17}O_{40}$,[11] $BaTiO_3$,[12,13] and Ba_2TiO_4,[14] only the last is not based on a close-packed {O,Ba/O} layer system. It contains isolated TiO_4 tetrahedra, making it quite distinct in the series. The phase $Ba_2Ti_5O_{12}$ was found to be stabilized by small amounts of impurities, and is therefore not a true polytitanate.[15] The framework structure of $Ba_4Ti_{11}O_{26}$ is related to the mineral jeppite,[16] but with partial occupancy of titanium to achieve charge balance (also referred to as $Ba_2Ti_{5.5}O_{13}$).[17]

The barium hexaferrite system and spinels differ markedly from the polytitanates in that Fe occupies both octahedral and tetrahedral interstitial sites in the close-packed lattice. This results in sixfold octahedral and fourfold tetrahedral coordination, as well as fivefold trigonal-bipyramidal coordination in the case of the hexaferrites. This last form is obtained when two tetrahedral interstitial sites share a face. The occupying iron atom is usually shifted out of the basal plane into either one of the tetrahedral interstitial sites.

In the case of the hexaferrites, various superstructures based on hexagonal lattices with the *c* axis approaching 1000 Å have been reported.[18] Other phases in the $BaO-Fe_2O_3$ system may adopt structures that are not based on a close-packed lattice. $BaFe_2O_4$, for instance, adopts a "stuffed tridymite"-type structure,[19] while $Ba_2Fe_2O_5$ is reported to occur in a distorted perovskite-type superstructure.[20] $Ba_2Fe_6O_{11}$ may be regarded as intermediate between the tridymite-type structures and the close-packed structures, as a layer of edge-shared octahedra alternate with a partial stuffed tridymite-like framework of tetrahedra.[21]

The spinels and hexaferrites are used in nonreciprocal microwave devices. However, they have considerably lower dielectric constants than the barium polytitanates.

Combinations of the barium polytitanates and barium hexaferrites are of potential interest since they offer the possibility of high dielectric constants in a magnetic system. Depending on the concentration of Fe^{3+}, paramagnetic to ferri- or ferromagnetic systems would be expected. At low iron concentrations, good dielectric materials based on polytitanates, but with weak magnetism, would be likely. In contrast, a high iron concentration would be expected to

Table 1. Crystal structure data for phases

Compound	#L	Stacking sequence	Layer thickness [Å]	Space group	Lattice parameters [Å]	Remarks name (see Figure 1), ref.
$Fe_2O_3-TiO_2$						
Fe_2TiO_5				*Ccmm*	$a = 9.700$, $b = 3.720$, $c = 9.930$	pseudobrookite[44]
$BaO-Fe_2O_3$						
Fe_3O_4	6	$(c)_c$	2.32	$F\bar{4}3m$	$a = 8.384$	S (spinel)[45]
$BaFe_{12}O_{19}$	10	$(hhhcc)_2$	2.32	$P6_3/mmc$	$a = 5.893$, $c = 23.194$	M (hexaferrite)[7,24]
$Ba_2Fe_{14}O_{22}$	18	$(cchhhh)_3$	2.42	$R\bar{3}m$	$a = 5.860$, $c = 43.504$	Y[7]
$BaFe_{18}O_{27}$	14	$(hhhcccc)_2$	2.34	$P6_3/mmc$	$a = 5.880$, $c = 32.845$	W[7]
$Ba_3Fe_{26}O_{41}$	22	$(hhhcchhhcc)_2$	2.38	$P6_3/mmc$	$a = 5.885$, $c = 52.301$	Z (MY)[7]
$Ba_2Fe_{30}O_{46}$	36	$(hhhcchhhcccc)_3$	2.306	$R\bar{3}m$	$a = 5.880$, $c = 84.110$	M_2S[7]
$BaFe_4O_7$	6	$(cch)_2$		$P6_3/m$	$a = 5.160$, $c = 13.811$	[46]
$BaFe_2O_4$	4	$(ch)_2$	2.254	$P6_322$	A = 5.458, $c = 9.016$	[19]
$BaO-TiO_2$						
cubic-$BaTiO_3$	3	$(c)_3$	2.306	$Pm\bar{3}m$	$a = 3.905$	[12]
6H-$BaTiO_3$	6	$(cch)_2$	2.327	$P6_3/mmc$	$a = 5.750$, $c = 14.050$	[13][31]
$Ba_6Ti_{17}O_{40}$	8	$(hcch)_2$	2.340	$C2/c$	$a = 9.883$, $b = 17.080$, $c = 18.920$, $\beta = 98.40°$	[11]
$Ba_4Ti_{13}O_{30}$	6	$(hcc)_2$	2.342	$Cmca$	$a = 17.063$, $b = 9.864$, $c = 14.053$	[10]
$Ba_2Ti_9O_{20}$	6	$(hhc)_2$	2.349	$P\bar{1}$	$a = 14.358$, $b = 14.095$, $c = 7.477$, $\alpha = 95.5°$, $\beta = 100.6°$, $\gamma = 89.9°$	[8]
$BaTi_5O_{11}$	6	$(hcc)_2$	2.337	$P2_1/n$	$a = 7.670$, $b = 14.020$, $c = 7.520$, $\beta = 98.3°$	[47]
$BaTi_6O_{13}$	4	$(h)_4$	2.377	$P\bar{1}$	$a = 7.510$, $b = 9.852$, $c = 7.461$, $\alpha = 105.2°$, $\beta = 118.5°$, $\gamma = 72.3°$	[48]
$Ba_2Ti_{13}O_{22}$	6	$(cch)_2$	2.349	$Cmca$	$a = 10.018$ $b = 11.575$, $c = 14.094$	[30]
$BaTi_2O_5$		–	–	$A2/m$	$a = 9.409$, $b = 3.932$, $c = 16.907$, $\beta = 103.5°$	framework[49]
$BaTi_4O_9$		–	–	$Pmmn$	$a = 14.527$, $b = 3.794$, $c = 6.293$	framework[50]
$Ba_2Ti_6O_{13}$		–	–	$C2/m$	$a = 15.004$, $b = 3.953$, $c = 9.085$, $\beta = 98.01°$	framework[51]
$BaO-Fe_2O_3-TiO_2$						
$Ba_2Fe_2Ti_4O_{13}$		–	–	$C2/m$	$a = 15.216$, $b = 3.898$, $c = 9.135$, $\beta = 98.46°$	A,[52] framework
$Ba_3Fe_{10}TiO_{20}$		–	–	$I2/m$	$a = 15.379$, $b = 11.837$, $c = 5.1845$, $\beta = 91.237°$	B,[32] framework
$BaFe_4Ti_2O_{11}$	6	$(h)_6$	2.264	$P6_3/mmc$	$a = 5.843$, $c = 13.604$	1:2:2[38]
$Ba_{12}Fe_{28}Ti_{15}O_{84}$	8	$(cchc)_2$	2.365	$C2/m$	$a = 9.988$, $b = 17.298$, $c = 19.170$, $\beta = 99.33°$	12:14:15[39]
$Ba_4Fe_2Ti_{10}O_{27}$	8	$(cchh)_2$	2.346	$C2/m$	$a = 19.870$, $b = 11.449$, $c = 9.909$, $\beta = 109.19°$	C[32]
$Ba_6Fe_{45}Ti_{17}O_{106}$	8	$(ch)_4$	2.338	$C2/m$	$a = 19.39$, $b = 20.26$, $c = 10.076$, $\beta = 105.27°$	D[42]
$BaFe_{11}Ti_3O_{23}$	8	$(ch)_4$	2.355	$C2/c$	$a = 19.561$, $b = 8.661$, $c = 10.120$, $\beta = 105.62°$	D′[42]
$Ba_4Fe_4Ti_3O_{16}$	10		2.374		$a = 5.7618$, $c = 23.738$	E
$Ba_4Fe_{28}Ti_5O_{56}$	5	$(chcch)$	2.359	$C2/m$	$a = 10.032$, $b = 17.441$, $c = 12.235$, $\beta = 105.43°$	F[40]
$Ba_4Fe_{28}Ti_5O_{56}$	10	$(chcch)_2$	2.366	$C2/c$	$a = 10.024$, $b = 17.378$, $c = 24.627$, $\beta = 106.15°$	F′[40]
$Ba_{11}Fe_2Ti_{26}O_{66}$	10	$(ccchh)_2$	2.332	$C2/c$	$a = 23.321$, $b = 11.384$, $c = 9.847$, $\beta = 90.09°$	G[34]
$Ba_5Fe_4Ti_{10}O_{31}$	18	$(chhhhhhhc)_2$	2.346	$P6_3/mmc$	$a = 9.9886$, $c = 42.226$	I[41]
$Ba_{27}Fe_{16}Ti_{33}O_{117}$	54	$(cchcchhhhcchhhhcch)_3$	2.354	$R\bar{3}m$	$a = 5.750$, $c = 127.10$	J[37]
$Ba_8Fe_{10}Ti_8O_{39}$	26	–	2.362	–	$a = 9.977$, $c = 61.41$	K[1]
$Ba_6Fe_4Ti_7O_{26}$	42	–	2.353	–	$a = 5.736$, $c = 98.84$	L[1]
$Ba_{11}Fe_8Ti_9O_{41}$	26	$(chcchchcchc)_2$	2.365	$P6_3/mmc$	$a = 5.754$, $c = 61.482$	M[35]
$Ba_2Fe_2Ti_2O_9$		–	–	–	–	N[1]

yield magnets, albeit with reduced dielectric constants. Superexchange, the prevalent magnetic interaction in insulating oxides,[22] produces antiferromagnetic spin alignments, reducing the overall possible magnetic moment of the material. Since the X-ray contrast between Fe and Ti is small, investigations studying the ordering of Fe and Ti may

need the use of synchrotron radiation tuned to the Fe or Ti absorption edge, or neutron diffraction experiments. High-resolution electron microscopy may also be utilized to study the ordering of Fe in such pseudo-quaternary phases.[23]

3. Structural Units

The structural motifs observed in the hexaferrites and the barium polytitanates are few, and so allow classification of the large variety of structures observed in these systems. Stacking sequences, on the other hand, may extend over many layers in one direction. Table 1 compiles the unit cell parameters and stacking sequences for various phases present in the $BaO-Fe_2O_3-TiO_2$ system. The structural motifs observed in the pseudobinary systems are briefly discussed here.

The following color scheme has been adopted for the representation of structures: barium atoms: green or yellow spheres; tetrahedral iron: red tetrahedron; pentagonal iron: gold bipyramid; octahedral iron: dark blue octahedron; octahedral titanium: light blue octahedron.

3.1. Spinel-Type Layers (S-Block)

The spinel-type structure of Fe_3O_4 is based on a close-packed oxygen lattice, with iron present in tetrahedral and octahedral interstitial sites. It should be noted that Fe_3O_4 is a mixed valent system, and so does not meet the criterion of Fe^{3+} ions only. However, since its structural features are prominent, it is described separately here. The layer stacking is $(c)_n$. There are two distinct layers: one with edge-sharing octahedra (sP1 layer), and the other with a 1:2 combination of octahedra and tetrahedra, connected through the corners (sP2 layer) (Figure 2). Three layers, stacked sP2−sP1−sP2, form an "S-block", of Fe_3O_4 stoichiometry with an average layer thickness of 2.33 Å.

3.2. Magnetoplumbite-Type Layers (R-, T-, and Q-Block)

Barium hexaferrite $BaFe_{12}O_{19}$, crystallizes in the magnetoplumbite-type structure,[7,24] containing spinel-type S- and R-blocks. The R-block incorporates pentagonal iron, found in a trigonal bipyramid sandwiched between spinel (sP1) layers. The position of the iron atom in the basal plane of the pyramid is unstable, resulting in displacements that move the iron atom into one of the oxygen tetrahedra in a random way. Two face-sharing FeO_6 octahedra and one barium atom complete the R-block unit. The close-packed oxygen lattice in the R-block has an $(h)_3$ stacking sequence, which gives an overall stacking sequence for the magnetoplumbite-type of $(hhhcc)_2$ (ten-layer structure) with an average layer thickness of 2.318 Å. The individual layers are shown in Figure 2. $BaFe_{12}O_{19}$ is also referred to as hexaferrite M, on the basis of phase diagram studies by Smit and Wijn.[25,7]

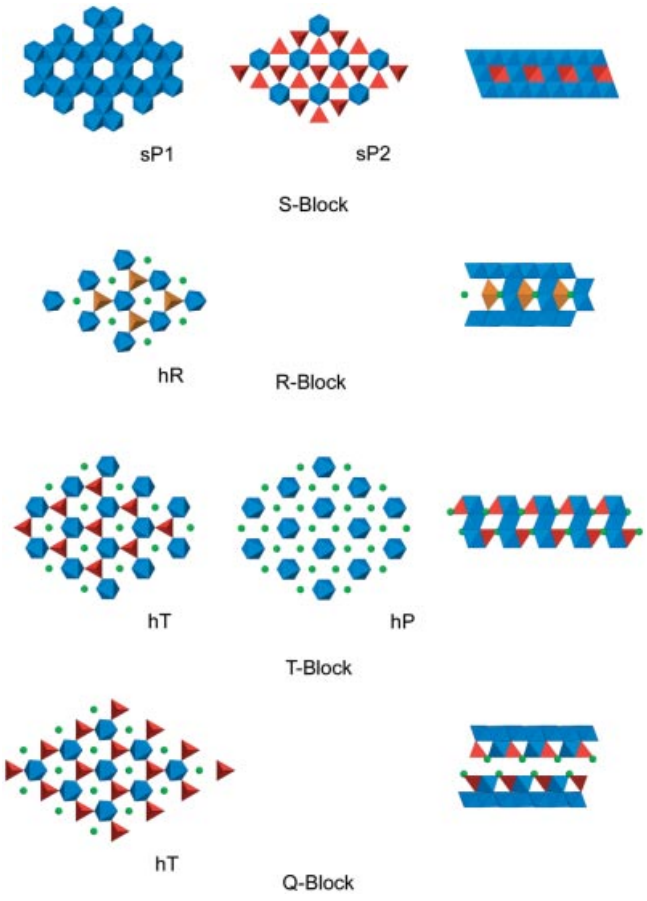

Figure 2. Close-packed layers found in spinel and hexaferrite phases; barium atoms are shown as green spheres, iron octahedra are indicated in dark blue, iron tetrahedra in red, and trigonal bipyramids in gold; the hexaferrites are made up of five different layers only

In hexaferrite Y, $Ba_2Fe_{14}O_{22}$ ($Ba_2Zn_2Fe_{12}O_{22}$),[25] a combination of S-blocks and T-blocks is observed. The T-blocks are made up of three close-packed layers (see Figure 2) containing columns of three face-sharing octahedra. The iron−iron distances in these columns are of the order of 2.84 Å, so iron atoms are moved out of their ideal positions. These iron−iron contacts allow only three face-sharing octahedra, since shifts in a fourth octahedron would be too large. The hT layer (Figure 2) may be regarded as a spinel sP2 layer in which all of the down-pointing tetrahedra have been removed, and a barium atom replaces the apical oxygen. The middle layer hP, containing Ba and octahedra only, is of the same type as observed in the cubic and hexagonal perovskite. The T-block may also be described as a modified R-block, in which the two tetrahedra forming the bipyramids are separated by a layer of octahedra, and are rotated by 60°.

The Q-block, found in iron and chromium ferrites, is related to the T-block in such a manner that the octahedral interstitial sites in the middle layer are not occupied (Figure 2).[26,27] A large number of hexaferrite phases can be described on the basis of the combinations of Q-, R-, S-, and T-blocks. Apart from $BaFe_{12}O_{19}$ (M),[28] for instance,

the hexaferrite phases $BaFe_{18}O_{27}$ (W), $Ba_2Fe_{14}O_{22}$ (Y), $Ba_3Fe_{26}O_{41}$ (Z), and $Ba_2Fe_{30}O_{46}$ (M_2S)[7] have been reported. With the exception of $BaFe_{12}O_{19}$, they show reduced iron valence, and are stabilized by the introduction of divalent atoms such as zinc, magnesium, or cobalt, or of mixtures such as Li^{1+}/Fe^{3+}. Some of these phases, with their stacking sequences and combinations of R-, S-, and T-blocks, are illustrated in Figure 3. For instance, $Ba_2Fe_{30}O_{46}$ is structurally a combination of $BaFe_{12}O_{19}$ and $BaFe_{18}O_{27}$, representing the M2S member, with block arrangement ($RSRS_2$).

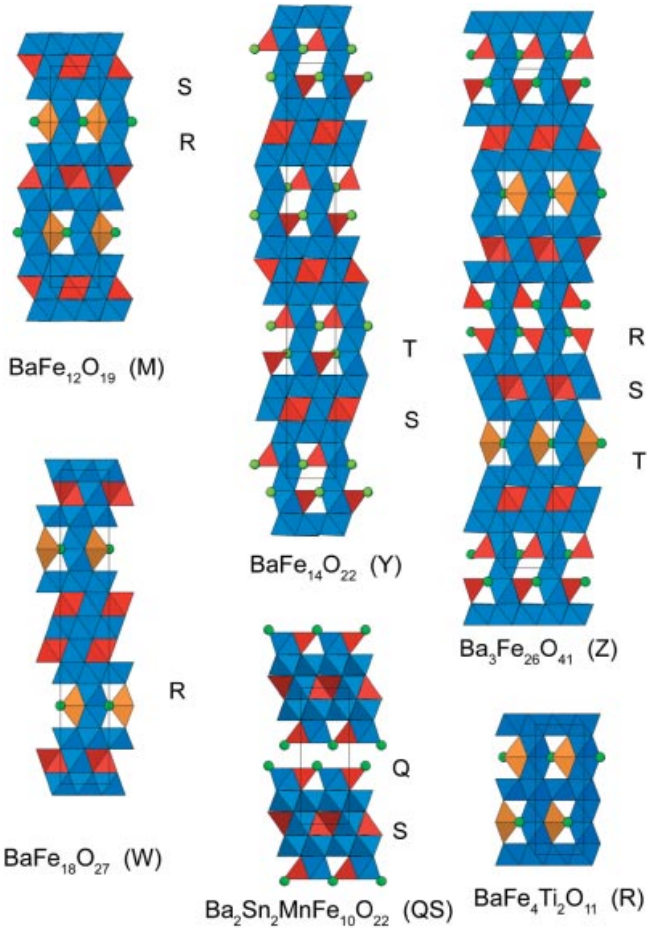

Figure 3. View of stacking sequences of hexaferrite phases M, W, Y, Z, and QS; barium atoms are shown as spheres, iron octahedra are indicated in blue, tetrahedra in red, and bipyramids in gold; hexaferrite building blocks shown in Figure 2 are indicated

The long-period superstructures observed may be described as stacking of different blocks in various ways, combinations, and periodicities.

3.3. Barium Polytitanates

The $BaO-TiO_2$ system contains a large number of phases, nearly all of which feature structures based on close-packed {O,Ba/O} lattices.[6] Mixed-valent barium titanate phases containing Ti^{3+}/Ti^{4+} mixtures have also been prepared and characterized; examples are the hollandite-type $Ba_2Ti_6O_{13}$[29] and the hexagonal 6L $Ba_2Ti_{13}O_{22}$.[22,30]

Only the cubic and hexagonal barium polytitanates are considered below, since these systems are based on close-packed {O,Ba/O} layers and tetravalent titanium in octahedral interstitials. Reduced titanium, Ti^{3+}, detrimentally affects the microwave properties. Barium titanate phases are compiled in Table 1.

The simplest structure present in the $BaO-TiO_2$ system is the well-known cubic perovskite $BaTiO_3$.[12] It may be regarded as a cubic stacking of close-packed layers with a thickness of 2.306 Å, a value expected to be close to the lower limit, since only corner-connected octahedra are present. Projection of the structure along one of the four close-packed stacking directions {111} shows the titanium octahedra well separated by barium atoms (Figure 4), and the same as the hP layer observed in the hexaferrite T-block.

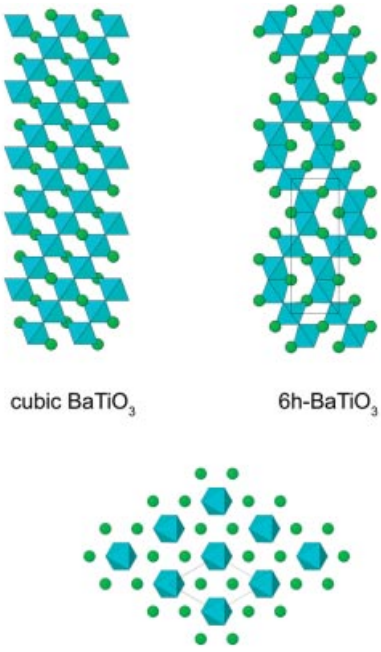

Figure 4. View of the stacking sequence for the cubic and hexagonal perovskite $BaTiO_3$; below is a depiction of a single perovskite layer, common to both structures; barium atoms are shown as green spheres, titanium octahedra are light blue, oxygen is found at the corners of the octahedra

The hexagonal 6H-$BaTiO_3$ structure[13,31] (Figure 4) has a stacking sequence $(cch)_2$ with an average layer thickness of 2.327 Å. It can be viewed as a cubic perovskite type, in which units of three layers are rotated by 180° and stacked on top of the previous layer, resulting in face-sharing titanium octahedra. The titanium−titanium distance in this double layer is increased from 2.327 to 2.69 Å, and so the metal atoms are moved away from the center of the octahedra. In general, face-sharing octahedra in titanates are observed in pairs, unlike in ruthenates, platinates, or nickelates, in which longer face-sharing chains of metal octahedra are found.[22] In an extended face-sharing arrangement, short Ti−Ti contacts of the order of 2.35 Å would be expected from the average layer thickness imposed by the oxygen−oxygen contacts, making such extended systems unstable.

The phases in the $BaO-TiO_2$ system may be written as $(BaO)_m(TiO_2)_n$, with $m = n = 1$ representing the simple $BaTiO_3$, with all tetravalent Ti. Alkaline earth rich titanates are not abundant, with Ba_2TiO_4 being the ($m = 2$, $n = 1$) phase, in which Ti is in tetrahedral coordination.[14] In contrast, a whole series of phases with ($m = 1$, $n = 2$, 4, 5, 6), ($m = 2$, $n = 5$, 9), ($m = 4$, $n = 11$, 13), and ($m = 6$, $n = 17$) have been reported and structurally characterized.[6] Most of these are based on close-packed {O,Ba/O} layers, with Ti in octahedral sites. The octahedra are connected through corners, edges, or faces, giving various stacking sequences. The framework structures of $BaTi_2O_5$, $BaTi_4O_9$, and $Ba_2Ti_{6-x}O_{13}$ (reduced) were discussed further by Tillmanns,[6] and are not considered further here.

Figure 5 shows the different close-packed layers found in $Ba_6Ti_{17}O_{40}$, $Ba_4Ti_{13}O_{30}$, $Ba_2Ti_9O_{20}$, $BaTi_5O_{11}$, and $BaTi_6O_{13}$.[6] The average layer thickness in these compounds is of the order of 2.34 Å. All these systems can be described in terms either of two or of three distinct topological layers. They combine edge- and corner-sharing octahedra only, without any face-sharing octahedra observed. The layers are often complementary in such a way that two or three layers cover an entire plane with octahedra by merging with shear, as for instance in $BaTi_6O_{13}$ and $BaTi_5O_{11}$, thus avoiding face-sharing octahedra.

It is interesting to note that $Ba_4Ti_{13}O_{30}$ [10] is the only phase in which the close-packed layers consist of discrete building blocks that do not form an extended unit. All the other phases have at least one close-packed layer with a one-dimensional chain-type building unit. The discrete building units within each plane are all of the same type; no combination of different units within a plane is observed for the polytitanates.

4. The $BaO-Fe_2O_3-TiO_2$ System

In contrast to the barium polytitanates, the barium hexaferrites show extended, two-dimensionally connected polyhedron arrays, generally resulting in higher symmetry structures. In combinations of the two systems, new types of intermediate structural building blocks would be expected. Indeed, exhaustive study of the $BaO-Fe_2O_3-TiO_2$ phase diagram revealed several new phases.[1] The nomenclature introduced in the phase diagram study is used below (Figure 1).

The five regions identified in the phase diagram are composed of: I. hollandites and framework structures (yellow); II. polytitanate-based systems (light blue); III. magnetic multilayer systems (blended hexagonal perovskite/hexaferrites(violet/gray); IV. hexaferrites and related phases, such as 1:2:2 (dark blue), and V. new family of mixed $BaO-Fe_2O_3-TiO_2$ phases (red).

4.1. Hollandites and Framework Structures (Yellow)

The systems based on framework-type structures are located near the titanium-rich corner of the phase diagram. The hollandite-type phases are in equilibrium with the framework-type phases 1:4 and A, the hexagonal systems 2:9, C and D, the pseudobrookite Fe_2TiO_5, and the hexaferrite-related 1:2:2.

4.2. Polytitanate-Based Systems (Light Blue)

The new phases C and G are in equilibrium with complex polytitanates, such as the phases 6:17 and 4:13, as well as with the cubic and hexagonal perovskites. Furthermore, phases C and G are in equilibrium with each other, which is reflected in the close structural relationship between them.

The layer stacking of phase C, $Ba_4Fe_2Ti_{10}O_{27}$,[32] and phase G,[33] $Ba_{11}Fe_2Ti_{26}O_{66}$,[34] is shown in Figure 6. The 8L structure of $Ba_4Fe_2Ti_{10}O_{27}$ is expanded into the 10L structure of $Ba_{11}Fe_2Ti_{26}O_{66}$ by repetition of the starting layer of every four-layer block. Phase G, $Ba_{11}Ti_{28}O_{66+x}$,[34] containing trivalent Fe, may be written as $Ba_{11}Fe_2Ti_{26}O_{66}$, but is likely to be intermediate, depending on preparation conditions such as oxygen partial pressure. It is easy to see that the close structural relationship of these two systems allows formation of intergrowths. Ordered superstructures based on the regular arrangement of blocks of four and five layers can produce a potentially large number of long-period superstructures. Further electron microscopy studies may reveal the presence of such ordered superstructures. In addition, both phases C and G introduce new close-packed layers in which, unlike in the pseudo-binary systems, two different building blocks are present within a layer. Isolated TiO_6 octahedra coexist with either Ti_5O_9 units or Ti_3O_{14} units.

4.3. Magnetic Super-Lattices (Blended Hexagonal Perovskites/Hexaferrites) (Violet/Gray)

The cubic and hexagonal perovskites $BaTiO_3$ are in equilibrium with the ternary phases A, C, E, G, I, J, K, L, M, N, and 12:14:15, as well as titanium-substituted barium hexaferrite. The new phases E, K, L, M, and N have previously been studied by high-resolution electron microscopy,[2] and further structural information is available for phases J and M. Alternating stacks of hexagonal perovskites and of layers preferentially occupied by Fe are common features in these phases. For instance, phase M, $Ba_{11}Fe_8Ti_9O_{41}$[35] (Figure 7), is a 26L structure with stacking sequence $[(cch)_3(ch)_2]$. As indicated, three hexagonal perovskite (*cch*) stacks alternate with four modified layers consisting of two octahedral layers and two spinel-related layers. All four of these modified layers preferentially contain Fe. Separated by nine hexagonal perovskite layers, this phase forms a natural magnetic super-lattice.[2,36] In the case of phase M, the magnetic layers are located around $z = 1/4$ and 3/4, spaced approximately 30.7 Å apart, with a hexagonal perovskite separation stack of the order of 21 Å in thickness. The iron-rich layers, however, show strong disorder. For instance, the layer containing tetrahedra, octahedra, and Ba may be described as an overlay of the hP and hT layers. The apparent densely packed layer of edge-sharing octahedra shows reduced metal occupancy, and may be regarded as a combination of spinel sP1 and hP layers.

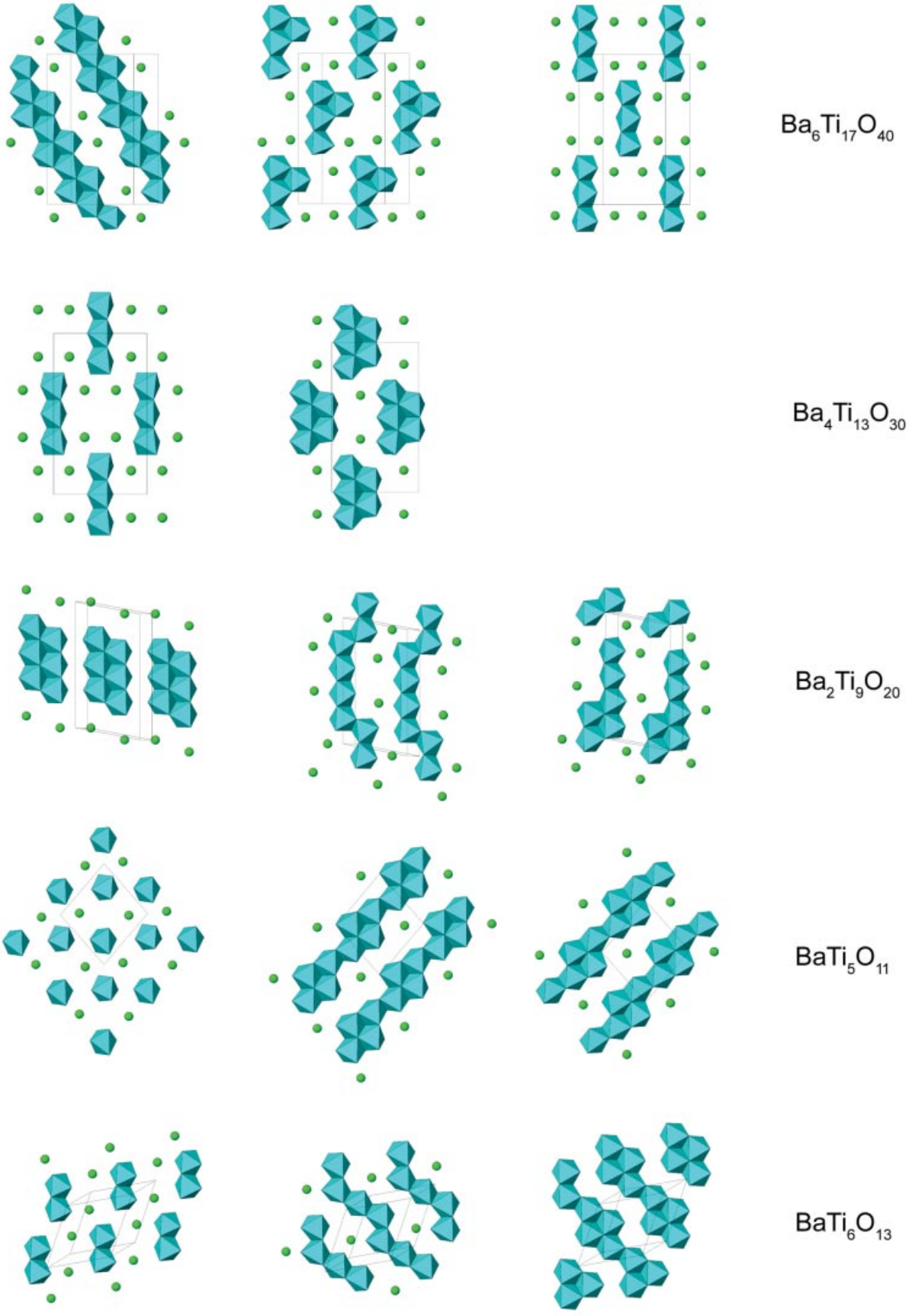

Figure 5. Compilation of the close-packed layers observed in hexagonal polytitanates; titanium octahedra are indicated in light blue and barium atoms are shown as green spheres; only $Ba_4Ti_{13}O_{30}$ has no extended building block

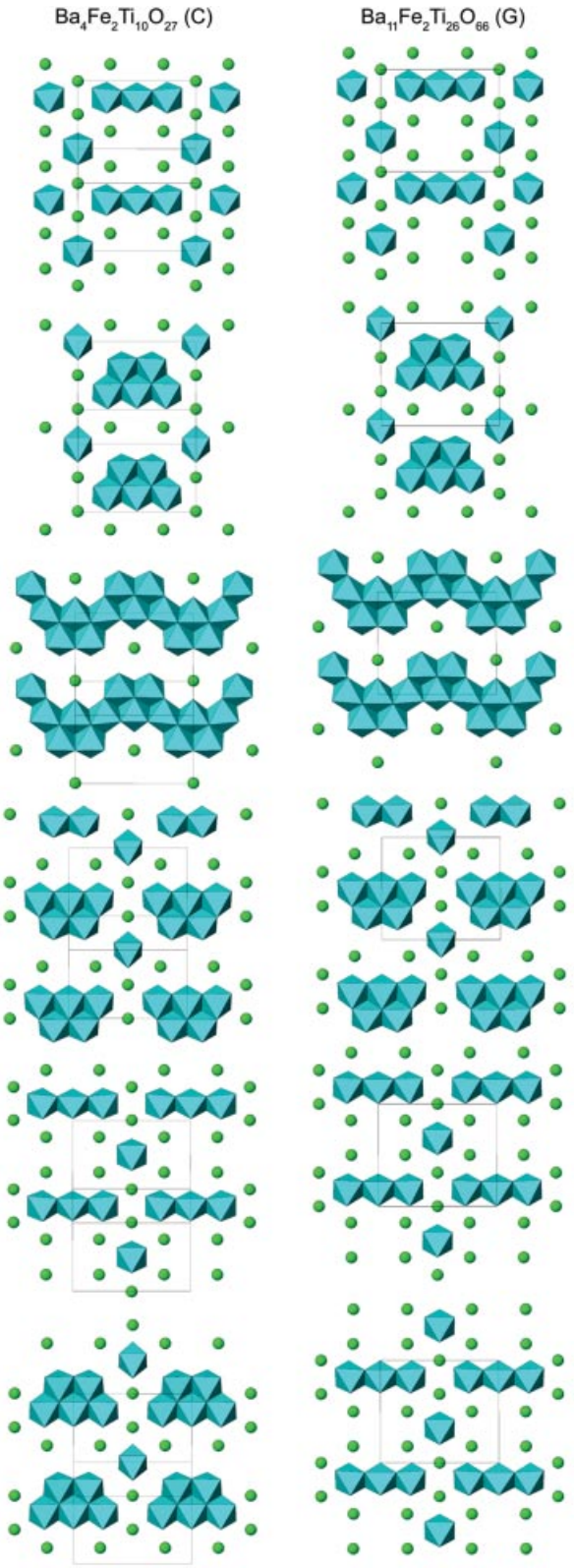

Figure 6. Close-packed layers of $Ba_4Fe_2Ti_{10}O_{27}$ (phase C) and $Ba_{11}Fe_2Ti_{26}O_{66}$ (phase G); the 8L structure of C is expanded into the 10L structure of G by repeating the starting layer in every four-block unit of phase C

Similarly, phase J (Figure 8), $Ba_{27}Fe_{16}Ti_{33}O_{117}$,[37] is based on the same building principle. It is a 54L structure with a $(cchcchhhhcchhhhcch)_3$ stacking sequence, previously described as an 18L monoclinic *C*-centered structure. Like phase M, it is a system with disorder and, to some extent, variable iron stoichiometry. As the stacking sequence indicates, the structure incorporates hexagonal perovskite (*cch*) blocks, alternating with iron-containing nine-layer blocks. Disorder similar to that in M, $Ba_{11}Fe_8Ti_9O_{41}$, is confined to those nine layers.[23,37] Furthermore, diffuse superstructure reflections observed in electron microscopy studies[2,36] indicate a possibly larger supercell.

While the structural characterization of phase E is not yet complete, preliminary investigations show that a hexagonal perovskite unit with a (*cch*) stacking sequence is again present, alternating with iron-containing layers. Furthermore, phases K, L, and N show similar building principles according to electron microscopy studies.[2] While the details of the structures need further elucidation, the overall building principle is well established, producing systems with magnetic iron blocks well separated by hexagonal perovskite blocks. These natural magnetic super-lattices may furthermore produce large supercells in which different blocks may be arranged in various ways. For instance, since J and L, as well as E and M, are in equilibrium, intergrowths are possible for these pairs of phases, giving rise to possible superstructures with *c* axes beyond 100 Å.

4.4. Hexaferrites and Related Phases (Dark Blue)

Phase 1:2:2, $BaFe_4Ti_2O_{11}$, is a hexaferrite-related system consisting of R-blocks only.[38] It is in equilibrium with phase 12:14:15, the framework-type phase A, the hollandites, and phases D and F. Interestingly, the magnetoplumbite $BaFe_{12}O_{19}$ is not in equilibrium with 1:2:2, despite the close structural relationship. Since the iron-only R-block $BaFe_6O_{11}$ has a net charge, the inclusion of two tetravalent titanium atoms renders the block neutral, resulting in the formation of phase 1:2:2. Similar stabilization might be expected from substitution of Zr^{4+} or Hf^{4+} for Fe.

Magnetoplumbite-type $BaFe_{12}O_{19}$ (hexaferrite M) has a solid solution range with TiO_2. It is in equilibrium with $BaFe_2O_4$, a hexagonal phase containing tetrahedral Fe only, Fe_2O_3, phases B, E, M, $Ba(Fe,Ti)O_3$, K, 12:14:15, D, and F. In Figure 1, the connection from the hexaferrites via the magnetic superlattice phases to the hexagonal perovskites is clearly seen. The large number of different types of hexaferrites, however, are not seen in the phase diagram since most of them require slightly reducing conditions upon preparation. The exception is phase 1:2:2, which is neutral. Intergrowths are to be expected on crystal chemical grounds, but are not observed in the phase diagram.

4.5. New Family of Ternary $BaO-Fe_2O_3-TiO_2$ Phases (Red)

New structures are found in the general transition-metal-rich part of the phase diagram, with an iron/titanium ratio ranging approximately from 4:1 to 1:2. These phases are characterized by the presence of fourfold tetrahedral and also fivefold bipyramidal Fe in new arrangements. The

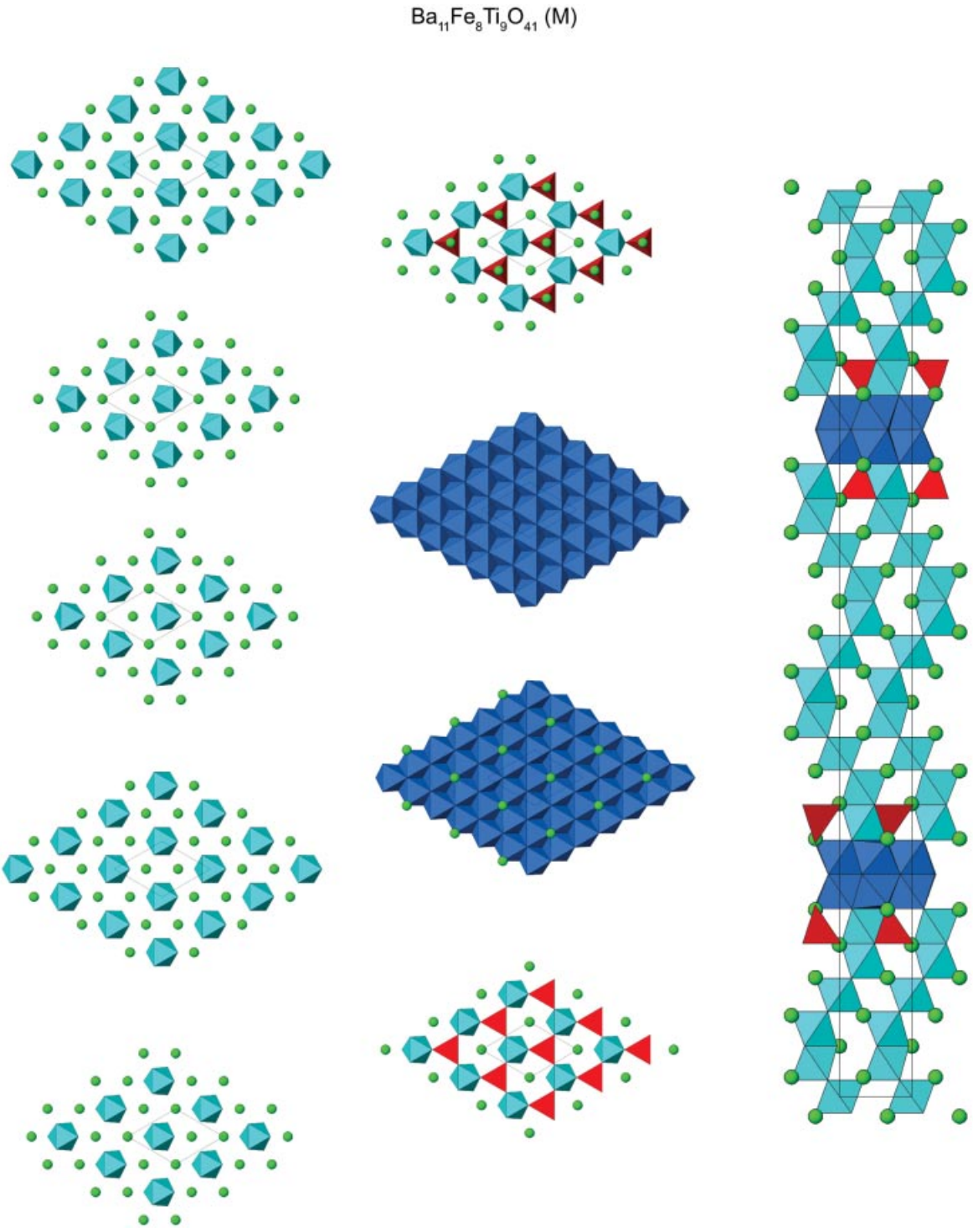

Figure 7. View of the close-packed layers and stacking arrangement of $Ba_{11}Fe_8Ti_9O_{41}$ (phase M), a 26L natural magnetic super-lattice in which iron-containing layers are separated by the hexagonal perovskite motif; disorder is confined to the iron-containing layers only, in which barium atoms randomly replace oxygen atoms; adjacent iron atoms show reduced occupancy corresponding to the barium occupancy factor

structural features show a strong relationship to spinel and magnetoplumbite. In the case of $Ba_{12}Fe_{28}Ti_{15}O_{84}$[39] there are five distinct layers, shown in Figure 9. There is a modified spinel-type layer (sP2) in which two tetrahedra are replaced by barium atoms (layer S1), and one in which five tetrahedra are replaced by barium atoms (layer S2). The latter may also be regarded as an hT layer in which two thirds of the tetrahedra have been removed. Layers containing octahedra only show symmetrical Ti_6O_{22} clusters made up of six edge-sharing octahedra (layer T1). Further,

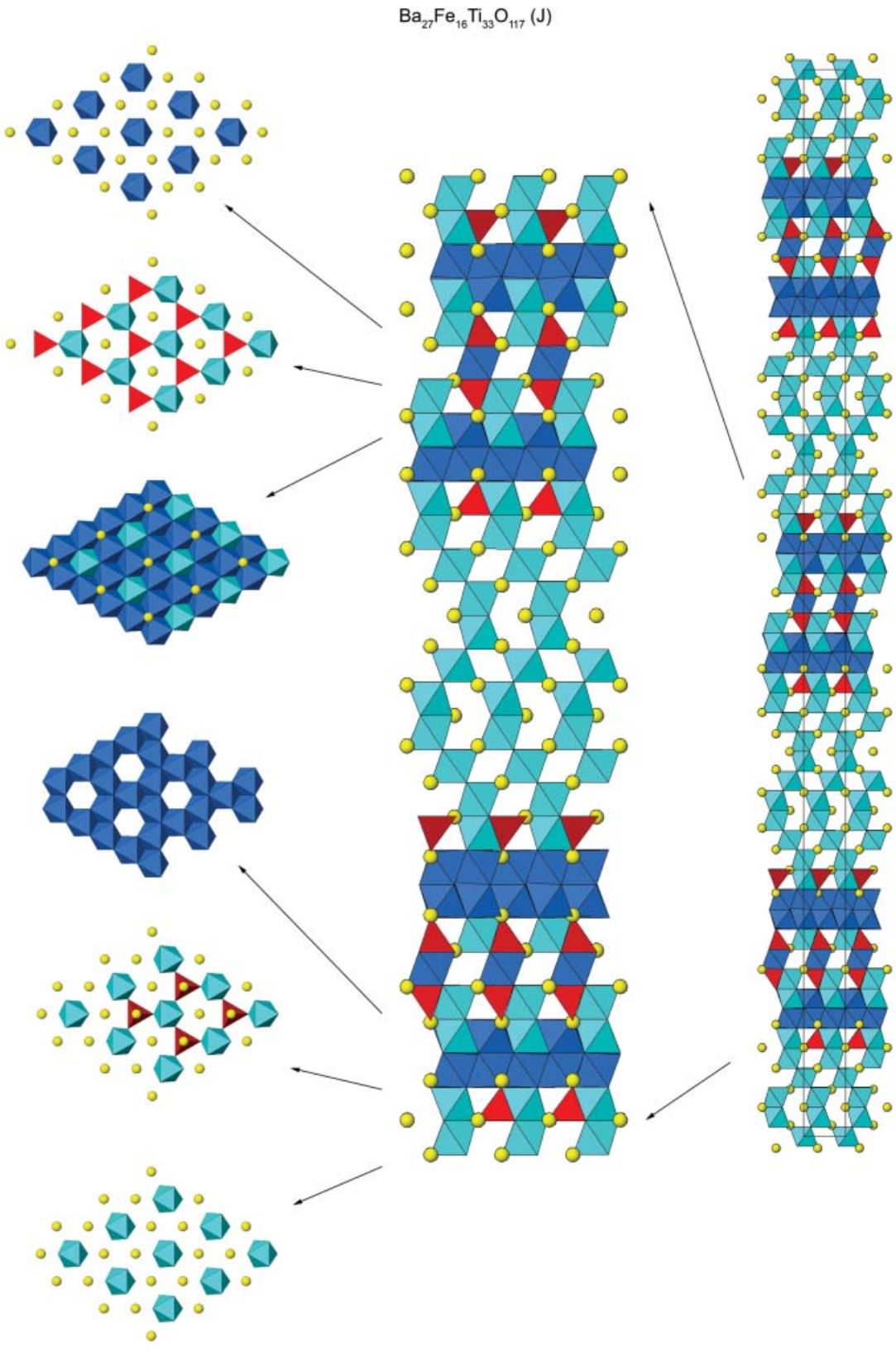

Figure 8. View of the close-packed layers and stacking arrangement of $Ba_{27}Fe_{16}Ti_{33}O_{117}$ (phase J), a 54L natural magnetic super-lattice; the rhombohedral structure has an 18L unique substructure with the hexagonal perovskite motif; disorder similar to that in phase M is observed in the iron-containing layers

layers with extended octahedron frameworks (T2), and finally hP perovskite-type-related layers in which half of the octahedra have been removed (layer P) make up the structure. These five different layer types produce the observed

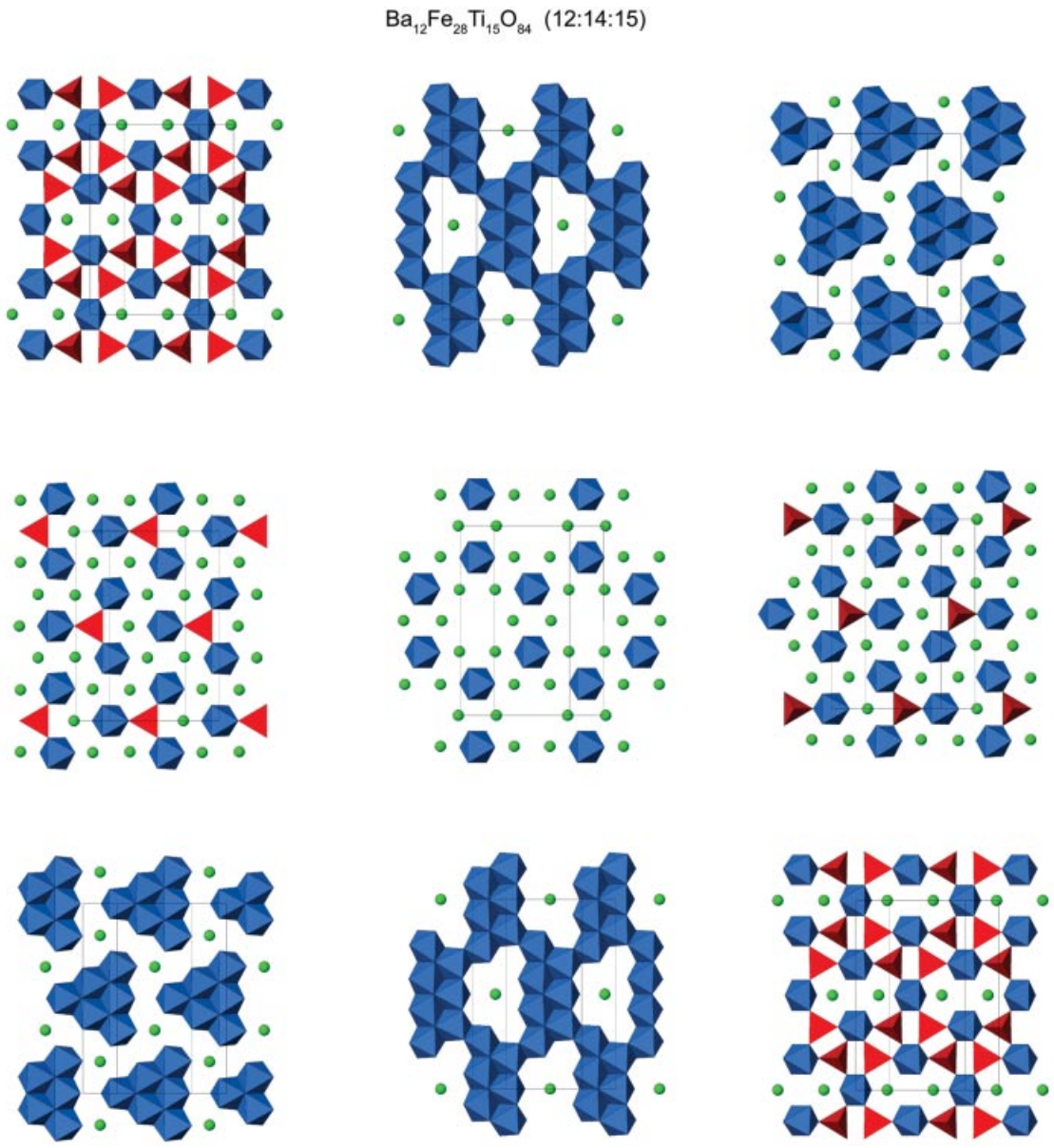

Figure 9. View of the close-packed layers of $Ba_{12}Fe_{28}Ti_{15}O_{84}$ (phase 12:14:15); four new layer types, intermediate between hexaferrite/spinel and polytitanate layers, are observed

8L structure with an {S1−T2−T1−S2−P−S2−T1−T2−S−...} stacking sequence.

The layers S1, T1, and T2 are again present in phase F, $Ba_4Fe_{28}Ti_5O_{56}$ (Figure 10),[40] in an {S1−T2−T1−T1−T2−S1−...} stacking sequence. Two modifications with this stacking were observed, the layers showing different relative orientations. The hexagonal symmetry of the T1 layer allows the orientation of the subsequent T2 layer to be changed by 120°. Superstructures with complicated stacking sequences are therefore possible for these systems. For instance, a more symmetrical unit cell may be produced by the stacking of 15 layers, with subsequent rotation of each five-layer block by 120°. Indeed, a unit cell indicating a 15L structure was previously observed for phase F.[1]

A further layer type is found in phase I, $Ba_5Fe_4Ti_{10}O_{31}$[41] (Figure 11), in equilibrium with $BaTiO_3$ and $Ba_2Fe_2Ti_4O_{13}$, as well as with $Ba_4Fe_2Ti_{10}O_{27}$ (phase C). Phase I is closely related to $Ba_{12}Fe_{28}Ti_{15}O_{84}$, with the S2 and T1 layers present, together with a modified T2′ layer. The T2′ layer derives from the T2 layer by removal of one octahedron to render the layer more symmetric. The combination of the T1 and T2′ layer again shows the principle of full plane coverage with two distinct layers, A new modified R-block of two close-packed layers R1 completes the 9L substructure found in this hexagonal 18L system. The modified R-block R1 shows a similar feature of substitution of barium for a tetrahedron, or, in this case a trigonal bipyramid. The resulting layers show a two-dimensional framework more open than the corresponding hexaferrite R-block.

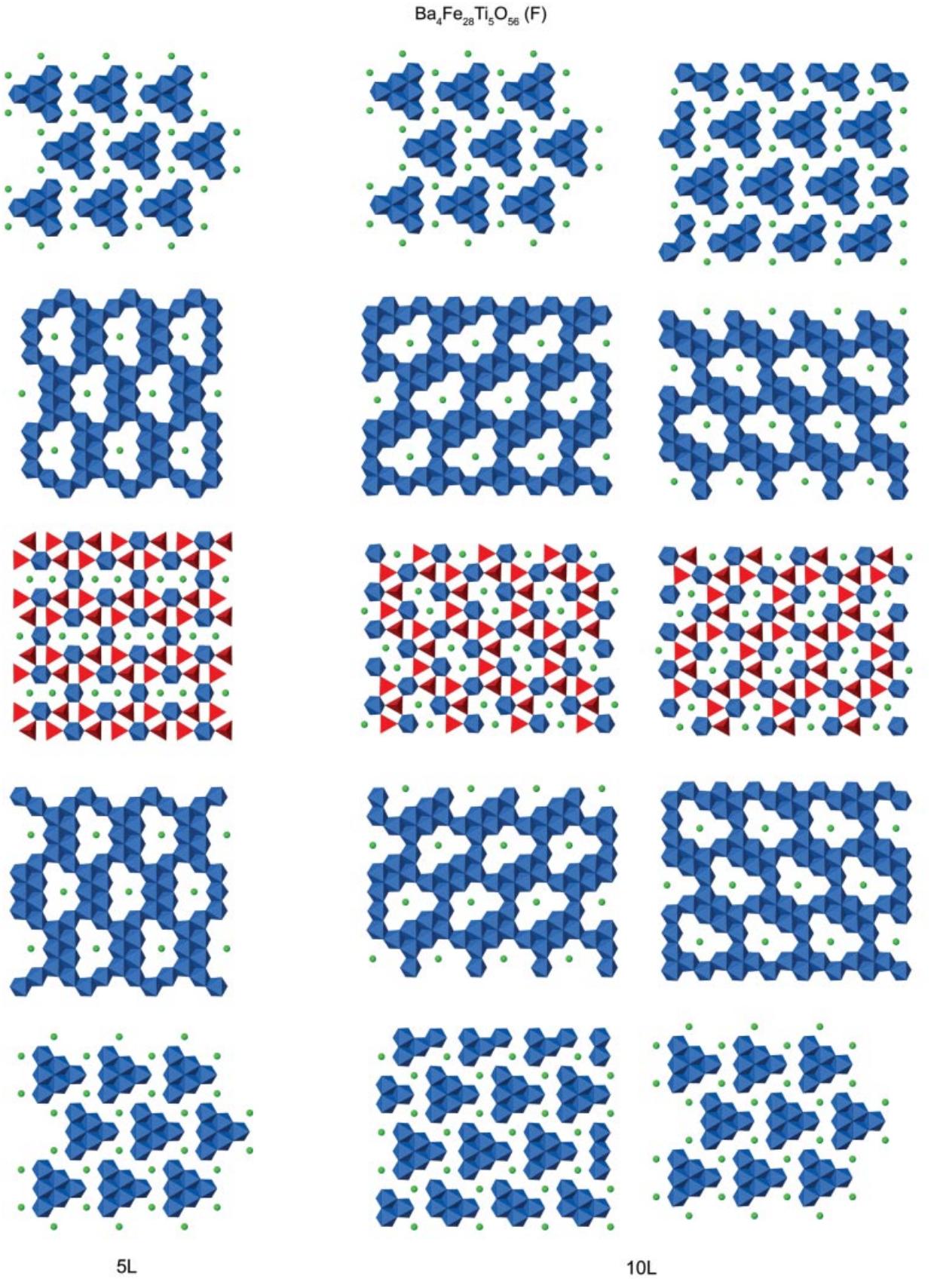

Figure 10. View of the close-packed layers of $Ba_4Fe_{28}Ti_5O_{56}$ (phase F); the 10L superstructure (right) can be derived from the 5L substructure (left) by rotation of the second layer depicted by 120°; only three of the five different layers of $Ba_{12}Fe_{28}Ti_{15}O_{84}$, are present, in the same relative arrangement

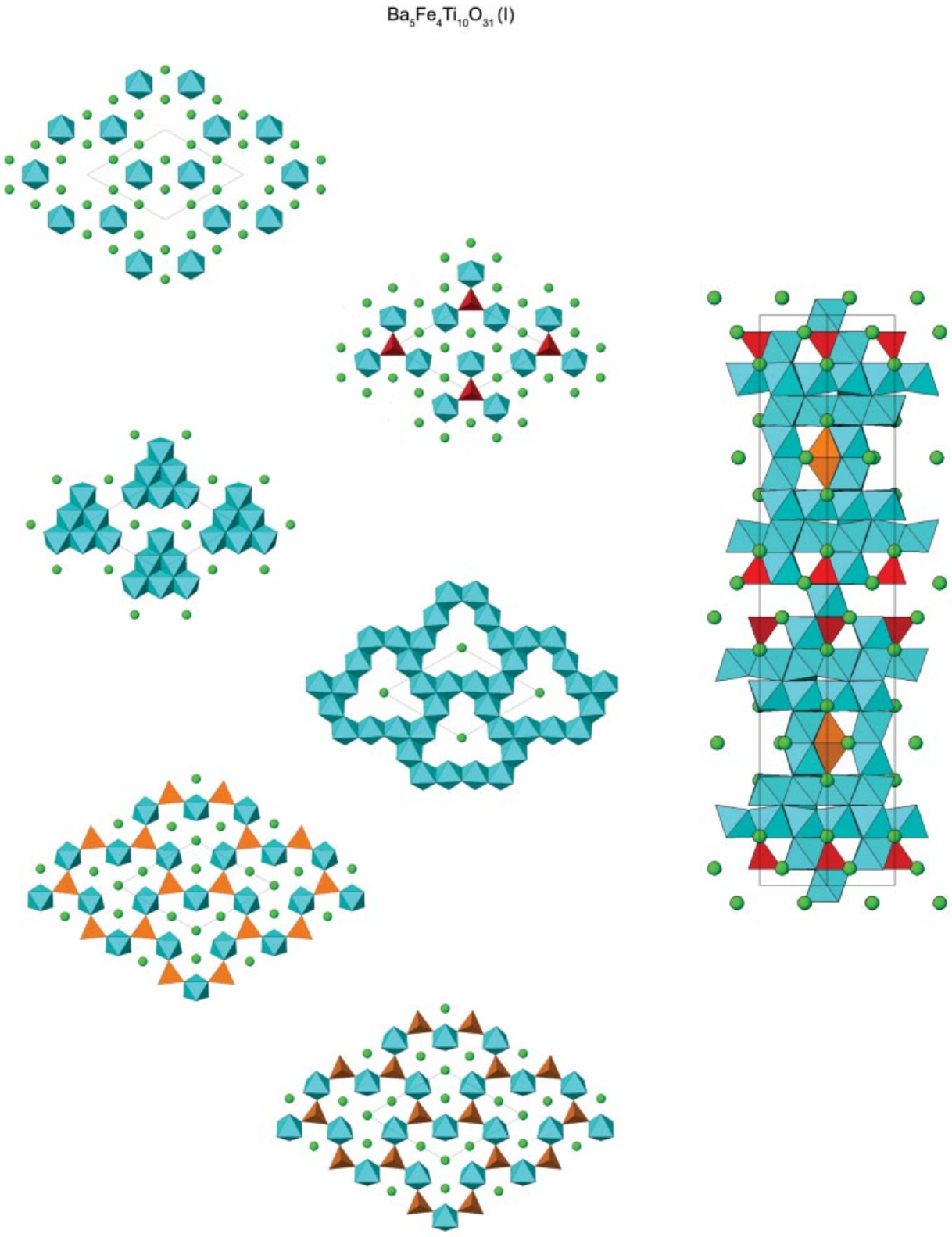

Figure 11. View of the close-packed layers and stacking arrangement of $Ba_5Fe_4Ti_{10}O_{31}$ (phase I); three of the six layers are identical to layers found in $Ba_{12}Fe_{28}Ti_{15}O_{84}$; furthermore, a modified R-block is seen

The stacking sequence in phase I is very similar to that in $Ba_{12}Fe_{28}Ti_{15}O_{84}$. In phase I, it is {P−S2−T1−T2′−R1−T2′−T1−S2−P−...}, in comparison with {P−S2−T1−T2−S1−T2−T1−S2−P−...}. In this respect, phase I ($Ba_5Fe_4Ti_{10}O_{31}$) may be regarded as a modified version of 12:14:15, $Ba_{12}Fe_{28}Ti_{15}O_{84}$. Unlike in

$Ba_{12}Fe_{28}Ti_{15}O_{84}$, the hexagonal symmetry is retained in $Ba_5Fe_4Ti_{10}O_{31}$, due to the higher symmetry of the R1 and T2′ layers, and the absence of the lower symmetric S1 layer. Even though the two structures are closely related in their crystal chemistry, they are not in equilibrium, and so intergrowth of the two would not be expected to occur under the given growth conditions. Interestingly, phase I displays an unusual barium coordination of 9+3 oxygen atoms in which the barium atom is shifted out of the close-packed plane, creating three short bonds of 2.74 Å and three long bonds of 3.50 Å.

A potentially large number of superstructures based on the various S1, S2, T1, T2, T2′, P1, and R1 layers (shown in Figure 12), may be envisioned. Furthermore, possible intergrowth structures produced under different growth conditions allow some degree of stoichiometric variation. Indeed, observed unit cells show lattice parameters up to about 40 Å, and larger superstructures are possible.

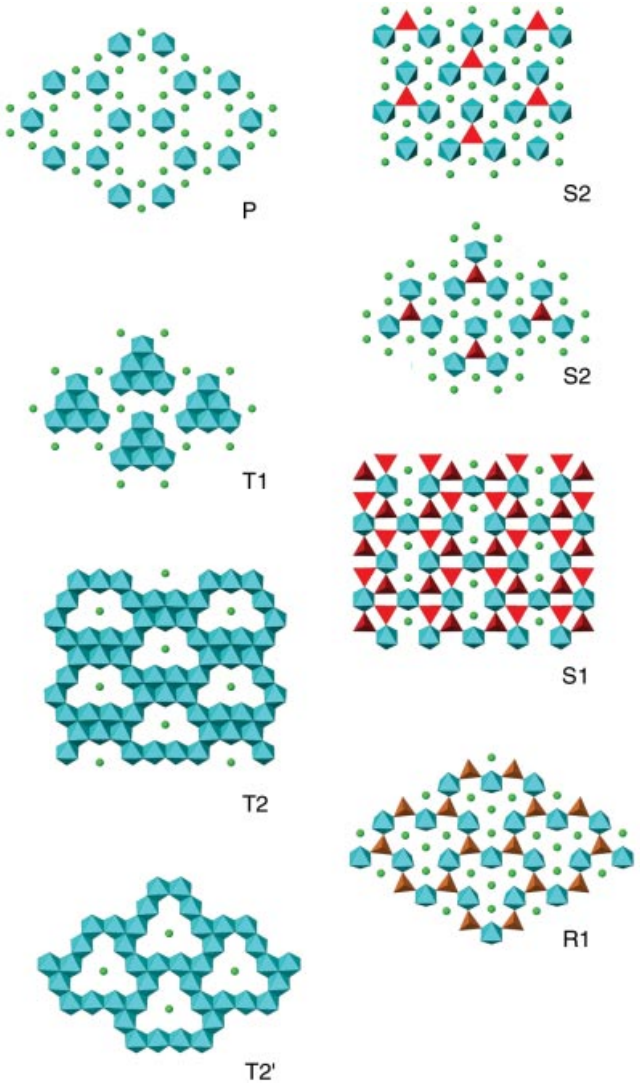

Figure 12. View of the seven different close-packed layers found in the new $BaO-Fe_2O_3-TiO_2$ phases; the close relationship to the T2 and T2′ layers can clearly be seen; the S1 and S2 layers are related to spinel-type layers, as are T2 and T2′ layers; the P and T1 layers are related to perovskite-type layers, and the R1 layers is related to the R-block layers in hexaferrite

Phases D, $Ba_6Fe_{45}Ti_{17}O_{106}$ and D′, $BaFe_{11}Ti_3O_{23}$, which are related,[42] are shown in Figure 13. The two distinct close-packed layers in phase D show a new building principle: the combination of different building units as described above within a single layer. For instance, a hexaferrite T-block layer composed of tetrahedra, octahedra, and Ba is combined with the previously described "ring" structure from a T2′ layer. Every second row of rings in the T2′ layer is split and expanded by the width of one octahedron to accommodate the three tetrahedra around an octahedron and the barium atom. In a similar way, the second layer is made up of the Ti_6O_{22} motif from the T1 layer in combination with the spinel-type sP1 layer of connected octahedra. In this respect, phase D may be regarded as a special intergrowth of the spinel-type structure and phase I, in which the combination is within the close-packed layers.

Phase D′, $BaFe_{11}Ti_3O_{23}$, is also composed only of two distinct layers (Figure 13). The structural motifs are related to the spinel-type structure, in which, in addition to Ba, the sP1 and sP2 layers are combined. As a result, phase D′ contains one-dimensional chains within a close-packed layer based on the substitution of barium for tetrahedra.

5. Dielectric Behavior

The dielectric response of a material may be described by use of the Clausius−Mosotti theory. This approach is valid for frequencies well below typical phonon frequencies in a solid-state material, and far from possible resonances due to magnetic atoms. In the case of the $BaO-Fe_2O_3-TiO_2$ system, Fe does not show resonance behavior up to frequencies of a few GHz. The dielectric constant ε of a material is related to the polarizability α and the molar volume V_m, with α being the sum over all the individual polarizabilities of the atoms in the molar volume ($\alpha = \Sigma_i \alpha_i$), according to Equation (1).

$$\varepsilon = \frac{1+\frac{8\pi\alpha}{3V_m}}{1-\frac{4\pi\alpha}{3V_m}} \quad (1)$$

The individual polarizabilities have been tabulated,[43] and give reasonable values for the dielectric constant ε. To achieve a high dielectric constant, it is therefore necessary to pack large atoms that are easily polarized in as small a volume as possible. As a guide, the value of $(4\pi\alpha/3V_m)$ should be close to 1.0. In the case of cubic $BaTiO_3$, this expression is approximately 0.9975, giving a calculated ε value of 1200. If $(4\pi\alpha/3V_m)$ is exactly 1.0, the expression diverges, giving a nonphysical value, and values larger than 1.0 would result in negative dielectric constants. The temperature dependence of the dielectric constant is related to the thermal expansion coefficient, since, to first order, only

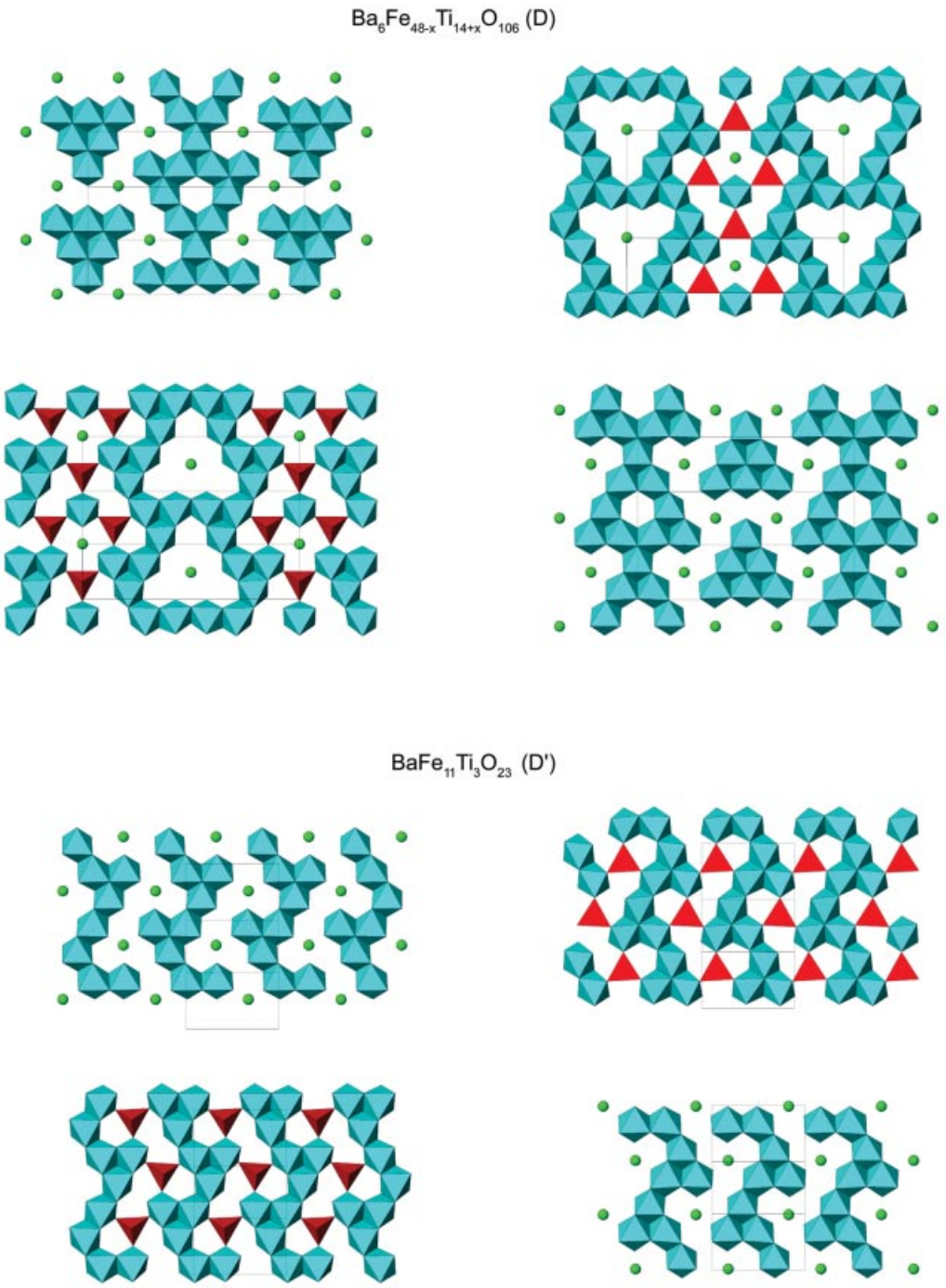

Figure 13. View of the close-packed layers in $Ba_6Fe_{48-x}Ti_{4-x}O_{106}$ (phase D, above) and $BaFe_{11}Ti_3O_{23}$ (phase D′, below); different building blocks are combined within a single close-packed layer; for instance elements of the T1 layer combines with the T2 layers, and elements of the T2′ layer combine with sP1 spinel-type layers in $Ba_6Fe_{48-x}Ti_{14+x}O_{106}$ (phase D); similarly, the combination of spinel-type elements and barium atoms within single layers are also observed for $BaFe_{11}Ti_3O_{23}$

the molar volume V_m has a temperature dependence of the form $V(T) = V_0(1 + \beta T)$. For technological use, a vanishing temperature dependence of ε is desirable, therefore excluding isotropic materials. Lower symmetry systems offer the opportunity of smaller temperature dependence of the molar volume, in which an expansion in one direction may be offset by a contraction in an other direction, resulting in a small or even zero overall thermal volume expansion coefficient. The values for atomic polarizabilities given are:[43] barium (Ba^{2+}) 6.40 Å^3; iron (Fe^{3+}) 2.29 Å^3; titanium (Ti^{4+}) 2.93 Å^3; oxygen (O^{2-}) 2.01 Å^3.

With these values, reasonable estimates of the dielectric constants of the phases found in the $BaO-Fe_2O_3-TiO_2$ system are obtained, assuming that the transition elements are in their expected valence states (i.e., no reduced titanium or reduced/oxidized iron atoms are present).

Estimated dielectric constants ε of a few selected compositions are given in Table 2. The values for the various compounds indicate the expected trend of lower dielectric constant with higher iron concentration, due to the reduced polarizability of iron versus titanium. Furthermore, higher barium concentrations would also be expected to increase the dielectric constant, as is reflected in the higher ε seen in phase M, $Ba_{11}Fe_8Ti_9O_{41}$, for which the estimated ε is of the order of 46. However, these values represent an approximation and do not take into account any loss mechanisms that may arise from mixed iron valence or reduction of titanium during the synthesis of the material.

Table 2. Estimated dielectric constants of selected compositions

Compound	$\varepsilon_{est.}$
$BaFe_4Ti_2O_{11}$ (1:2:2)	30
$Ba_{12}Fe_{28}Ti_{15}O_{84}$ (12:14:15)	26
$Ba_2Fe_2Ti_4O_{13}$ (A)	11
$Ba_3Fe_{10}TiO_{20}$ (B)	10
$Ba_4Fe_2Ti_{10}O_{27}$ (C)	27
$Ba_6Fe_{45}Ti_{17}O_{106}$ (D)	25
$BaFe_{11}Ti_3O_{23}$ (D′)	23
$Ba_4Fe_{28}Ti_5O_{56}$ (F)	23
$Ba_{11}Fe_2Ti_{26}O_{66}$ (G)	31
$Ba_5Fe_4Ti_{10}O_{31}$ (I)	33
$Ba_{27}Fe_{16}Ti_{33}O_{117}$ (J)	46
$Ba_{11}Fe_8Ti_9O_{41}$ (M)	47

It is clear from the above that systems based on channel structures are in general less efficiently packed than close-packed structures, and so polarizabilities per molar volume tend to be smaller for the channel-type structures.

Since the polarizability of barium is roughly twice that of titanium and almost three times that of iron, it is possible to increase the dielectric constant by substituting Ba in place of an iron tetrahedron. This substitution principle has been observed in the phases discussed above, and is reflected in the higher dielectric constants, both estimated and observed, for the barium-rich systems. The highest concentration of Ba would be expected for BaO (cubic rock salt type), but the estimated dielectric constant is only of the order of 15. Here, the molar volume is markedly larger than in comparable $BaO-Fe_2O_3-TiO_2$ phases, due to the lattice contraction (reduction in molar volume) produced by the higher charge on the transition metal atoms in interstitial sites.

6. Magnetic Behavior

The magnetic properties of the new phases in the $BaO-Fe_2O_3-TiO_2$ system are not yet fully established. However, the ferrimagnetic behavior of the hexaferrites is well known and documented.[25]

In the $BaO-Fe_2O_3-TiO_2$ phases as prepared, iron is present as Fe^{3+}, the desired valence state for low loss behavior. Free trivalent Fe is in a $^6S_{5/2}$ state, with a free magnetic moment of 5.92 μ_B. In cases of spinels and hexaferrites, the individual magnetic moments for trivalent iron are the full spin-only moment of 5.92 μ_B, but the magnetic superexchange produces antiferromagnetic coupling between the iron sub-lattices, reducing the net magnetic moment. Superexchange tends to produce antiferromagnetic spin alignments, although more complicated spin structures are possible.[22] Furthermore, the crystal field may produce low-spin iron. All these effects tend to reduce the overall magnetic moment per formula unit. Dilution of iron with nonmagnetic titanium induces changes in the magnetic coupling while reducing the number of spins. In special cases, an increase in the magnetic moment is possible if strong antiferromagnetic coupling is reduced.

At low iron concentrations, paramagnetic behavior with antiferromagnetic interactions would be expected, as observed, for instance, in the case of $Ba_5Fe_4Ti_{10}O_{31}$. Here, paramagnetic behavior was observed at room temperature, with cooperative interactions apparent below 250 K, but without magnetic order at low temperatures.[41] The effective magnetic moment per iron atom, obtained from the high-temperature susceptibility, is 5.12 μ_B, close to the free-atom value. The negative Weiss constant of $\Theta = -190$ K indicates that the dominant interactions are antiferromagnetic in nature. Furthermore, possible magnetic cluster formation is reflected in the behavior of the susceptibility.

Similarly, $Ba_6Fe_{45}Ti_{17}O_{106}$ (phase D) shows Curie–Weiss behavior, with a high-temperature effective magnetic moment of 34 μ_B per formula unit (45 iron atoms), and $\Theta = -806$ K, indicating strong antiferromagnetic interactions. A magnetic transition below 100 K was observed, and was attributed to a small amount of a strongly magnetic impurity, such as $BaFe_{12}O_{19}$. In comparison with $Ba_{12}Fe_{28}Ti_{15}O_{84}$,[39] a phase with less overall iron that shows a ferromagnetic Curie temperature well above room temperature, $Ba_6Fe_{45}Ti_{17}O_{106}$ is an exceptionally weak magnet. Appropriate chemical substitutions would be likely to improve magnetic properties by reducing the antiferromagnetic coupling between different sub-lattices.

The natural magnetic super-lattices found in the regions with low overall iron content merit further investigation, since the iron atoms are preferentially found near to one another. In this way, magnetic interactions within the layers may occur at higher temperatures than might be expected from the overall iron concentration alone. In addition, the two-dimensional character of the structure should be reflected in its magnetic behavior.

7. Conclusions and Outlook

The $BaO-Fe_2O_3-TiO_2$ system shows a wealth of new phases with interesting structural, dielectric, and magnetic properties. The crystal chemistry of a majority of the phases in this system is based on close-packed structures made up of {O,Ba/O} layers. With relatively few distinct types of layers, combining octahedra, tetrahedra, trigonal bipyramids, and barium atoms, a rich variety of stacking sequences with different combinations of the various layers

are found. In the polytitanate-related phases, new types of layers with complexity intermediate between that of the hexaferrites and that of polytitanates form. As in the hexaferrites, superstructures with long periodicities develop, all based on a few common types of layers (Figures 2, 5, and 12). Furthermore, preferential ordering of Fe in distinct layers well separated from each other produces natural magnetic super-lattices. Relationships between structures, based on the stacking arrangement of similar layers in various ways, can be identified in the $BaO-Fe_2O_3-TiO_2$ system. In contrast to the barium polytitanates, which often show low crystallographic symmetry, the mixed barium hexaferrites tend to exhibit higher symmetries based on hexagonal features.

The polarizability of iron is smaller than that of titanium, and substitution of Fe for Ti reduces the overall dielectric constant. This is offset in part by the ability of Fe to occupy tetrahedral interstitial sites, allowing a higher concentration. Phases with high dielectric constants are therefore observed in the mixed iron/titanium systems.

Most microwave materials in use today are composite materials, so knowledge of the phase diagram provides crucial processing information. Combination of hexaferrites and barium polytitanates in a composite process should produce phases described above. Since properties are additive in ceramic composites, knowledge of physical and chemical properties is crucial for tailoring of a material to maximize its performance.

The large number of new phases observed in the $BaO-Fe_2O_3-TiO_2$ phase diagram has produced new insights into the crystal chemistry of these phases. Since the cut of the phase diagram was carried out at 1275 °C, more phases are likely under different preparation conditions. So far, the presence of Fe^{3+} has been needed for microwave applications. However, reduced oxygen pressures may stabilize other new, as yet unknown phases. The rich crystal chemistry observed in this system may be expected to extend into related phases, prepared under different synthesis conditions.

Acknowledgments

We would like to thank L. Schneemeyer, L. Bendersky, and R. S. Roth for valuable discussion and comments.

[1] T. A. Vanderah, J. M. Loezos, R. S. Roth, *J. Solid State Chemistry* **1996**, *121*, 38.
[2] L. A. Bendersky, T. A. Vanderah, R. S. Roth, *Philos. Mag. A* **1998**, *78*, 1299.
[3] G. Geiger, *Am. Ceram. Soc. Bull.* **1994**, *73*, 57.
[4] T. Abraham, *Am. Ceram. Soc. Bull.* **1994**, *73*, 62.
[5] *Phase Equilibria Diagrams* (formerly *Phase Diagrams for Ceramists*), Am. Ceram. Soc., Westerville, OH, **1964**, **1975**, **1981**, **1991**, **1993**, **1995**, **1996**.
[6] E. Tillmanns, W. Hofmeister, W. H. Baur, *J. Solid State Chem.* **1985**, *58*, 14.
[7] P. B. Braun, *Philips Res. Rep.* **1957**, *12*, 491.
[8] E. Tillmanns, W. Hofmeister, W. H. Baur, *J. Am. Ceram. Soc.* **1983**, *66*, 268.
[9] D. H. Templeton, C. H. Dauben, *J. Chem. Phys.* **1960**, *32*, 1515.
[10] E. Tillmanns, W. H. Baur, *Inorg. Nucl. Chem. Lett.* **1971**, *7*, 1169.
[11] E. Tillmanns, W. H. Baur, *Acta Crystallogr., Sect. B* **1970**, *26*, 1645.
[12] H. D. Megaw, *Nature* **1945**, *155*, 484.
[13] H. Blattner, H. Gränicher, W. Känzig, W. Merz, *Helv. Phys. Acta* **1948**, *21*, 341.
[14] K. K. Wu, I. D. Brown, *Acta Crystallogr., Sect. B* **1973**, *29*, 2009.
[15] R. S. Roth, J. J. Ritter, H. S. Parker, D. B. Minor, *J. Am. Ceram. Soc.* **1986**, *69*, 858.
[16] H. Cid-Dresdner, M. Buerger, *Z. Kristallogr., Kristallgeom., Kristallphys., Kristallchem.* **1962**, *117*, 411.
[17] W. Hofmeister, E. Tillmanns, *Fortschr. Mineral.* **1978**, *56*, 42.
[18] A. F. Wells, *Structural Inorganic Chemistry*, Clarendon Press, Oxford, **1975**.
[19] S. Meriani, *Acta Crystallogr., Sect. B* **1972**, *28*, 1241.
[20] X. D. Zou, S. Hovmoeller, M. Parras, J. M. Gonzales-Calbet, M. Vallet-Regi, J. C. Grenier, *Acta Crystallogr., Sect. A* **1993**, *39*, 27.
[21] C. Boivin, D. Thomas, G. Pouillard, P. Perrot, *J. Solid State Chem.* **1979**, *29*, 101.
[22] J. B. Goodenough, J. M. Longo, in: *Landolt-Börnstein*, vol. III/4a new series (Ed.: K.-H. Hellwege), Springer Verlag, Berlin, Heidelberg, New York, **1970**, p. 126.
[23] L. A. Bendersky, T. A. Vanderah, R. S. Roth, *Mat. Res. Soc. Symp. Proc.* **1997**, *453*, 489.
[24] X. Obradors, A. Collomb, M. Pernet, D. Samaras, J. C. Joubert, *J. Solid State Chem.* **1985**, *56*, 171.
[25] J. Smit, H. P. J. Wijn, *Ferrites*, John Wiley & Sons, and Philips Technical Library, New York and Eindhoven, **1959**.
[26] M. C. Cadee, H. J. M. de Groot, L. J. de Jongh, D. J. W. Ijdo, *J. Magn. Magn. Mater.* **1986**, *62*, 367.
[27] I. S. Hagemann, Q. Huang, X. P. A. Gao, A. P. Ramirez, R. J. Cava, *Phys. Rev. Lett.* **2001**, *86*, 894.
[28] W. D. Townes, J. H. Fang, A. J. Perotta, *Z. Kristallogr., Kristallgeom., Kristallphys., Kristallchem.* **1967**, *125*, 11.
[29] W. H. Baur, E. Tillmanns, W. Hofmeister, *Cryst. Struct. Commun.* **1982**, *11*, 2021.
[30] S. Möhr, H. K. Müller-Buschbaum, *J. Alloys Compd.* **1993**, *199*, 203.
[31] I. E. Grey, C. Li, L. M. D. Cranswick, R. S. Roth, T. A. Vanderah, *J. Solid State Chem.* **1998**, *135*, 312.
[32] T. A. Vanderah, W. Wong-Ng, Q. Huang, R. S. Roth, R. G. Geyer, R. B. Goldfarb, *J. Phys. Chem. Solids* **1997**, *58*, 1403.
[33] R. S. Roth, C. J. Rawn, C. G. Lindsay, W. Wong-Ng, *J. Solid State Chem.* **1993**, *104*, 99.
[34] T. Siegrist, T. A. Vanderah, personal communication, **2000**.
[35] T. Siegrist, C. Svensson, T. A. Vanderah, R. S. Roth, *Solid State Sci.* **2001**, *2*, 539.
[36] L. A. Bendersky, J. E. Bonevich, *Philos. Mag. Lett.* **1998**, *77*, 279.
[37] T. Siegrist, T. A. Vanderah, C. Svensson, R. S. Roth, *Solid State Sci.* **2002**, *4*, 911.
[38] F. Haberey, M. Velicescu, *Acta Crystallogr., Sect. B* **1974**, *30*, 1507.
[39] I. E. Grey, A. Collomb, X. Obradors, *J. Solid State Chem.* **1991**, *91*, 131.
[40] T. Siegrist, T. A. Vanderah, personal communication, **2000**.
[41] T. Siegrist, T. A. Vanderah, A. P. Ramirez, R. G. Geyer, R. S. Roth, *J. Alloys Compd.* **1998**, *274*, 169.
[42] T. A. Vanderah, W. Wong-Ng, B. H. Toby, V. M. Browning, R. D. Shull, R. G. Geyer, R. S. Roth, *J. Solid State Chem.* **1999**, *143*, 182.
[43] R. D. Shannon, *J. Appl. Phys.* **1993**, *73*, 348.
[44] M. Hamelin, *Bull. Soc. Chim. Fr.* **1958**, 1559.
[45] W. H. Bragg, *Nature* **1915**, *95*, 516.
[46] S. I. Okamoto, T. Ito, *Acta Crystallogr., Sect. B* **1973**, *29*, 832.

[47] E. Tillmanns, *Acta Crystallogr., Sect. B* **1969**, *25*, 1444.
[48] E. Tillmanns, *Cryst. Struct. Commun.* **1972**, *1*, 1.
[49] E. Tillmanns, *Acta Crystallogr., Sect. B* **1974**, *30*, 2894.
[50] W. Hofmeister, E. Tillmanns, W. H. Baur, *Acta Crystallogr., Sect. B* **1984**, *40*, 1510.
[51] W. Hofmeister, E. Tillmanns, *Acta Crystallogr., Sect. B* **1979**, *35*, 1590.
[52] T. A. Vanderah, Q. Huang, W. Wong-Ng, B. C. Chakoumakos, R. B. Goldfarb, R. G. Geyer, J. Baker-Jarvis, R. S. Roth, A. Santoro, *J. Solid State Chem.* **1995**, *120*, 121.

Received June 21, 2002
[I02338]